Available online at www.sciencedirect.com
ScienceDirect
Journal of the European Ceramic Society 31 (2011) 2463–2470
www.elsevier.com/locate/jeurceramsoc

Synthesis of CeO_2–ZrO_2 solid solution by glycothermal method and its oxygen release capacity

Saburo Hosokawa, Seiichiro Imamura, Shinji Iwamoto, Masashi Inoue *

Department of Energy and Hydrocarbon Chemistry, Graduate School of Engineering, Kyoto University, Katsura, Kyoto 615-8510, Japan

Available online 2 March 2011

Abstract

The glycothermal (GT) reaction of Ce acetate and Zr alkoxide directly yielded CeO_2–ZrO_2 solid solutions in a region of low Ce content ≤40 mol%. Of the CeO_2–ZrO_2 solid solutions obtained by the GT method and subsequent calcination at 500 or 800 °C, the sample with 20 mol% Ce content had the largest BET surface area. This sample exhibited the highest Ce-based oxygen release capacity in the whole Ce/Zr composition range. The oxygen release capacities of CeO_2–ZrO_2 solid solutions synthesized by the GT method were much larger than those of the samples prepared by a coprecipitation (CP) method. The Reitveld analysis and the repetitive reduction–oxidation experiment indicated that the CeO_2–ZrO_2 solid solution synthesized by the GT method has a homogeneous structure as compared with that prepared by the CP method.

Keywords: CeO_2; ZrO_2; Chemical properties; Thermal properties; Glycothermal method

1. Introduction

The CeO_2–ZrO_2 solid solution is an important oxygen-storage component for the use in automobile catalysts.[1–4] It has been reported that the oxygen storage capacity (OSC) is generated by interconversion between Ce^{4+} and Ce^{3+} under oxidative and reductive conditions.[5,6] The OSC of the CeO_2–ZrO_2 solid solution depends largely on the method of preparation; many physical properties such as crystallinity, crystallite and particle sizes, and homogeneity change depending upon its preparation methods and, thus, influence the OSC,[7] and many methods such as solid-state reaction,[8] high-energy milling,[9] coprecipitation method,[10,11] sol–gel method,[12,13] citrate complex method,[14] polymerized complex method,[15] combustion synthesis,[16,17] and hydrothermal method[4,18] have been reported.

We have been exploring the method for synthesizing inorganic materials in organic media at elevated temperatures. Various mixed oxides are directly crystallized when two suitable starting materials in the forms of alkoxide, acetylacetonate, acetate, etc. are allowed to react in glycol at 200–300 °C (glycothermal reaction).[19–22] In most cases, the use of 1,4-butanediol (1,4-BG) is essential for the formation of well-crystallized homogeneous products. In a previous paper, the reaction of mixtures of zirconium alkoxide and Ce acetate in 1,4-BG at 300 °C was reported to afford nano-crystalline tetragonal CeO_2–ZrO_2 solid solutions.[23] However, the properties of these solid solutions were investigated only for a limited Ce/Zr composition range.

Various synthetic methods closely related to the glycothermal one have been reported. Rumruangwong and Wongkasemjit[24] synthesized CeO_2–ZrO_2 solid solutions by hydrolysis of mixtures of cerium glycolate and sodium tris(glycozirconate) and subsequent calcination. In the glycothermal reaction, glycolates are possibly formed as intermediates; however, they are not hydrolyzed but thermally decomposed. Suda et al.[25] synthesized CeO_2–ZrO_2 solid solutions by calcination of the gel obtained by treatment of cerium and zirconium nitrates in ethylene glycol at 150 °C and reported the thus-obtained materials had high OSC values. Zhang et al.[26] reported the formation of nanocrystalline CeO_2–ZrO_2 solid solutions by thermal decomposition of cerium and zirconium acetylacetonates in oleylamine; however, the reducibility of their materials was not reported. Hydrothermal treatment of coprecipitated gels was reported to increase the thermal stability of the CeO_2–ZrO_2 solid solutions.[27,28]

In this work, CeO_2–ZrO_2 solid solutions were prepared by the glycothermal method with a wide composition range, and their OSC and physical properties were investigated in comparison

* Corresponding author. Tel.: +81 75 383 2478; fax: +81 75 383 2479.
E-mail address: inoue@scl.kyoto-u.ac.jp (M. Inoue).

0955-2219/$ – see front matter © 2011 Elsevier Ltd. All rights reserved.
doi:10.1016/j.jeurceramsoc.2011.02.009

with the CeO_2–ZrO_2 solid solutions obtained by a conventional co-precipitation method.

2. Experimental

2.1. Preparation of CeO_2–ZrO_2 solid solutions

2.1.1. Glycothermal method (GT)

Cerium acetate monohydrate and zirconium tetra-*n*-propoxide (Ce + Zr = 30 or 50 mmol) were suspended in 140 ml of 1,4-BG in a test tube; the tube was then placed in a 300-ml autoclave. An additional 40 ml of 1,4-BG was placed in the gap between the autoclave wall and the test tube. The autoclave was purged with nitrogen, heated to 300 °C at a rate of 2.3 °C/min, and maintained at that temperature for 2 h. After the assembly was cooled to room temperature, the resultant product was collected by centrifugation. The product was washed with methanol by vigorous mixing and centrifuging, and then air-dried.

2.1.2. Co-precipitation method (CP)

Cerium nitrate and zirconium oxynitrate (Ce + Zr = 20 mmol) were dissolved in 300 ml of deionized water. A hydroxide gel was precipitated from the solution at pH above 12 by adding 3 N NaOH. After the gel was stirred at room temperature for 1 h, it was filtered and washed with deionized water until the pH of the filtrate became <8, followed by drying at 90 °C overnight.

Both GT and CP samples were calcined at prescribed temperatures for 30 min unless otherwise specified. These samples are abbreviated as GT(x) or CP(x), where x stands for nominal molar content of ceria. If required, calcination temperature in degree Celcius is given after the abbreviation. For example, GT(20)-800 means the GT sample with 20 mol% Ce content calcined at 800 °C.

2.2. Characterization

The X-ray powder diffraction patterns (Shimadzu XD-D1 diffractometer) were recorded using CuKα radiation. The crystallite sizes of the CeO_2–ZrO_2 solid solutions were calculated from the half-height width of the 1 1 1 diffraction peak at ~30° according to Scherrer's equation. For Rietveld analysis, the XRD pattern was recorded on another diffractometer, Rigaku Rint 2500, and analyzed by a RIETAN-2000 program.[29] The TCH pseudo-Voigt profile function was used and parameters were optimized in the following order: the unit cell parameter, the fractional coordinate of oxygen, and then the partial substitution of Zr ions in the 2*a* sites with Ce ions. Specific surface areas were calculated by the BET single-point method on the basis of N_2 uptake measured at 77 K by the use of a sorptionmeter (Micromeritics Flowsorb II 2300). Morphologies of the solid solutions were observed using a Hitachi H-800 transmission electron microscope operated at 200 kV. Temperature-programmed reduction (TPR) was carried out with a flow-type reactor. Hydrogen (2 vol.% in Ar; 30 ml/min) was passed through the reactor charged with a sample (0.05 g) under atmospheric pressure. The reactor was heated with an electric furnace with a heating rate of 5 °C/min up to 950 °C, and the amount of H_2 consumed was monitored with a TC detector of a Shimadzu 4CPT gas chromatograph. In the repetitive reduction–oxidation experiment, the reduced catalyst after the first TPR run was re-oxidized with O_2 (20 vol.% in He) at 500 °C for 1 h and the second TPR run was performed after cooling to the room temperature. Atomic composition of the sample was determined by ICP atomic emission spectroscopy (AES; Shimadzu ICPS-1000IV) after the sample was dissolved in a hot mixture of H_2SO_4 and H_2O_2.

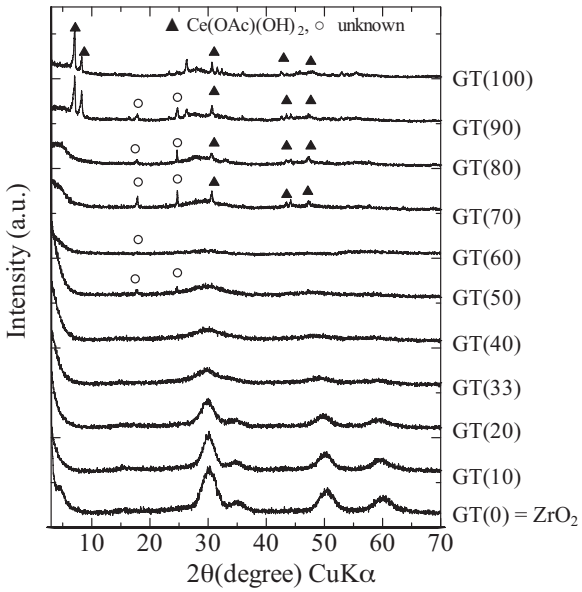

Fig. 1. XRD patterns of as-synthesized GT samples.

3. Results and discussion

The XRD patterns of the as-synthesized GT products are shown in Fig. 1. Tetragonal zirconia was formed for GT(0). With the increase in the Ce content, the diffraction peaks due to tetragonal zirconia shifted towards the lower angle side and were broadened. These results indicate that CeO_2–ZrO_2 solid solutions were directly formed by the GT reaction and that their crystallinity decreased with the increase in the Ce content. For GT(100) and GT(90), the diffraction peaks were assigned to $Ce(OAc)(OH)_2$,[30] although GT(90) exhibited peaks due to unknown phase(s). The samples with Ce contents of 50–80 mol% exhibited low intensity peaks due to the $Ce(OAc)(OH)_2$ and unknown phases, suggesting that these samples were essentially amorphous.

Fig. 2 shows the representative data for thermal analysis of the GT products. A significant weight loss was observed at 200–300 °C associated with an exothermic peak in DTA. The weight loss of GT(20) was much smaller than that of GT(80) and is due to the combustion of surface organic groups. It was reported that 4-hydroxybutyl groups are bound to the surface oxygen atoms of the GT products.[19] The large weight loss together with an intense exothermic peak observed for GT(80) suggests that a large amount of organic moieties are present in

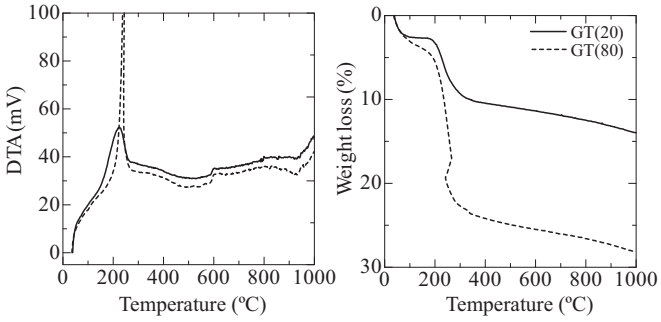

Fig. 2. TG-DTA profiles of as-synthesized GT(20) and GT(80) samples.

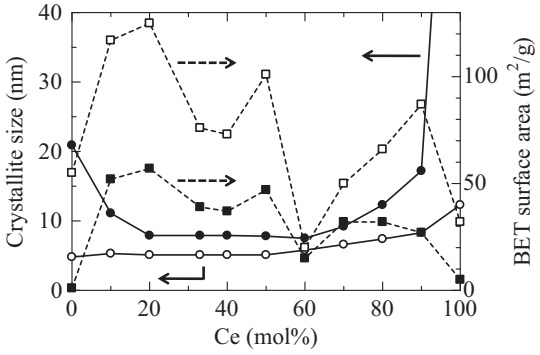

Fig. 4. Effects of Ce content on crystallite size (circle) and BET surface area (square) of GT samples calcined at 500 °C (open symbols) and 800 °C (closed symbols).

the framework of the product. Note that the theoretical weight loss due to the formation of CeO_2 from $Ce(OAc)(OH)_2$ is 26.2%.

Fig. 3 shows the XRD patterns of the calcined GT and CP products. The GT samples calcined at 500 °C showed symmetrical diffraction peaks, and with the increase in the Ce content, the peak positions shifted towards the lower angle side, suggesting that CeO_2–ZrO_2 solid solutions were formed in the whole composition range without segregation to CeO_2 and ZrO_2 phases. Although the as-synthesized GT products with Ce contents of 50–80 mol% were essentially amorphous (Fig. 1), solid solutions were formed by calcination at 500 °C, indicating that the amorphous phase was composed of homogeneously mixed Ce and Zr ions.

The pure ZrO_2 sample obtained by the GT method (GT(0)) partly transformed to monoclinic ZrO_2 on calcination at 800 °C (Fig. 3b). Although calcination of GT(10) at 800 °C produced a small amount of monoclinic ZrO_2 by phase segregation (datum not shown here), other GT samples did not show any indication of the phase segregation.

In the case of CP(50)-800, the diffraction peak apparently splitted into two peaks (Fig. 3c), suggesting that Ce and Zr ions are not homogeneously distributed in the CP samples as compared with the GT samples.

The effects of the composition on the crystallite size and BET surface area of the GT samples are shown in Fig. 4. The crystallite size of the sample calcined at 500 °C had a tendency to increase slightly with the increase in the Ce content. The samples with the Ce contents <60 mol% had the crystallite sizes of ~5 nm, while that of single-component CeO_2 was 12.3 nm. Calcination at 800 °C increased the crystallite size. The samples with 20–60 mol% Ce had the crystallite size of ~8 nm, and those of both the Ce-rich (Ce, >70 mol%) and Zr-rich (Ce <20 mol%) samples were much larger.

Roughly speaking, the BET profile exhibited two maxima, although the data were largely scattered. Similar phenomena have been frequently observed.[31,32] GT(20) had the largest surface area irrespective of the calcination temperature (125 and 57 m^2/g for GT(20)-500 and -800, respectively).

Fig. 5 shows the TEM images of the GT and CP samples obtained by calcination at 800 °C. Spherical particles with 1–2 μm diameter were observed for GT(20) (Fig. 5a), and its high-magnification image (Fig. 5b) indicated the spherical particles were composed of primary particles with ~10 nm size which is essentially identical with the crystallite size (8 nm). GT(60) and GT(80) were composed of irregularly shaped particles (Figs. 5c and d). The low surface areas of these GT samples seem to be due to their morphology. CP(20) was composed of irregularly shaped aggregates of fine primary particles.

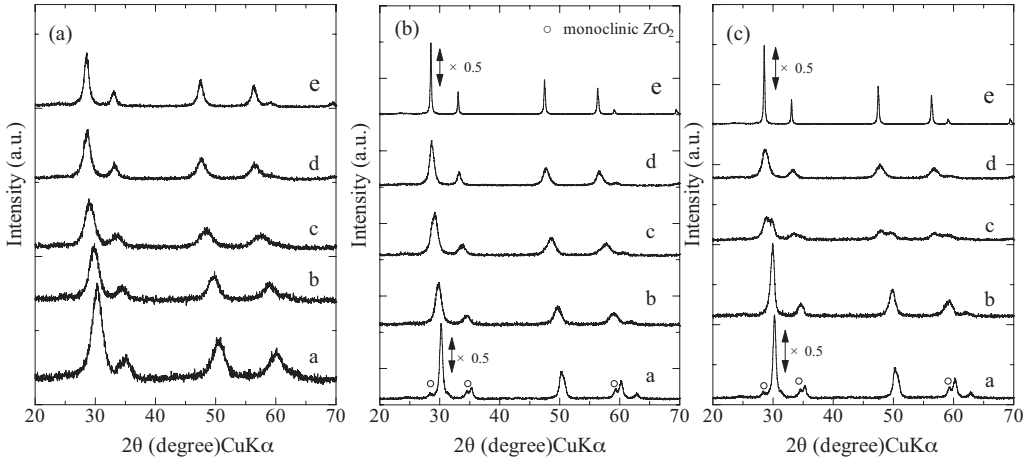

Fig. 3. XRD patterns of (a) and (b), GT samples obtained by calcination at (a) 500 and (b) 800 °C; for 30 min; and (c), CP samples obtained by calcination at 800 °C for 30 min. Ce mol%: a, 0 [ZrO_2]; b, 20; c, 50; d, 80; e, 100 [CeO_2].

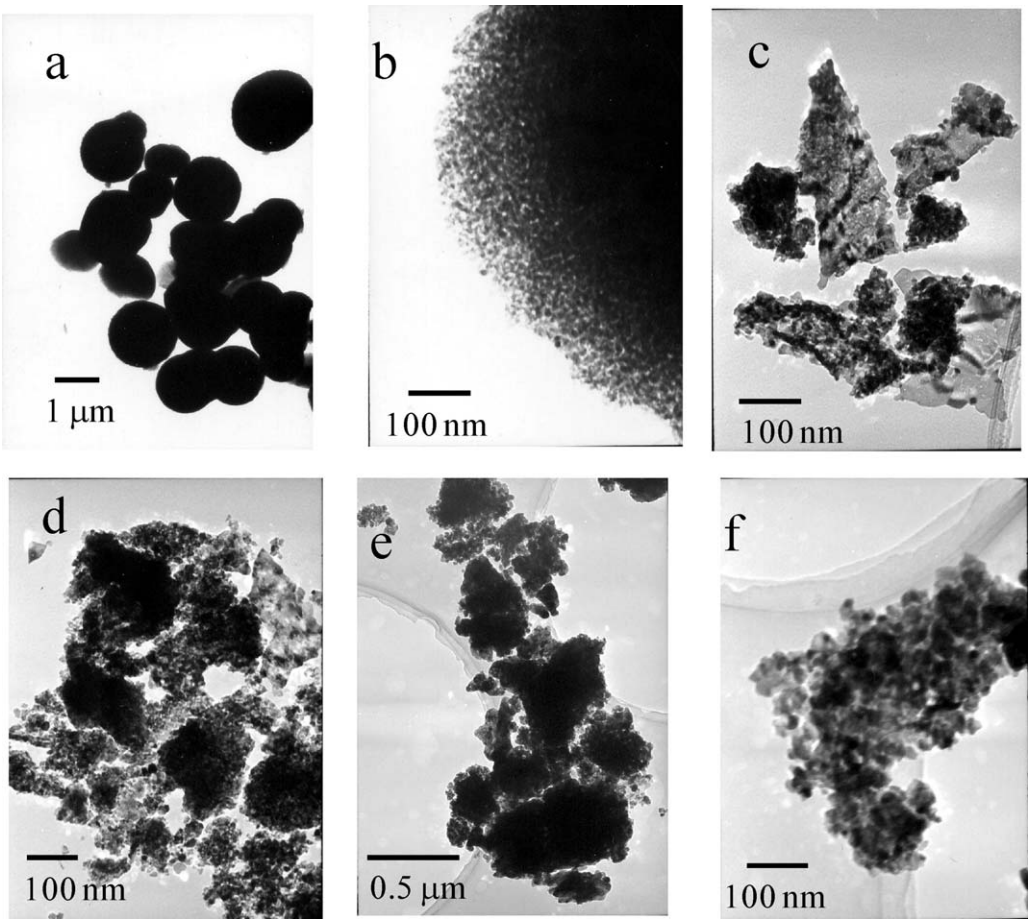

Fig. 5. TEM images of (a and b), GT(20)-800; (c), GT(60)-800; (d), GT(80)-800; (e and f), CP(20)-800.

Fig. 6 shows the TPR profiles of the GT and CP CeO_2–ZrO_2 solid solutions calcined at 800 °C. The GT samples with Ce content ≤60 mol% had only one reduction peak at 400–600 °C, while two peaks at 400–600 °C and >700 °C were observed for the samples with 60–90 mol% Ce contents (some data not shown in Fig. 6). Takeguchi et al. also observed a reduction peak at 350–600 °C for a CeO_2–ZrO_2 solid solution with 25 mol% of Ce which was prepared by the glycothermal method followed by calcination at 400 °C.[33]

CP(20) had a sharp peak at ∼260 °C in addition to a broad peak at 500 °C. However, the peaks of the samples with Ce content of 50–80 mol% were essentially identical with those of the GT samples.

Table 1 gives representative data for the quantity of H_2 consumed together with the BET surface area and crystallite size of the GT and CP samples calcined at 800 °C for 30 min or 3 h. These samples had surface areas of 30–57 m^2/g and crystallite sizes of 5–8 nm. For CP samples, the total H_2 consumption (the sum of H_2 consumptions at all the peaks) decreased with the decrease in Ce content. However, the total H_2 consumption was not proportional to the Ce content; the sample with low Ce content exhibited much larger H_2 consumption than that expected from the Ce content. Moreover, among the GT products, GT(50) showed the largest total H_2 consumption. Therefore, H_2 consumption per mole Ce was calculated, which increased with the decrease in the Ce content.

Another important feature that can be abstracted from Table 1 is that the GT samples consumed larger amounts of H_2 than the CP samples, and this point will be discussed later.

As shown in Fig. 6, the reduction peaks were classified into low- and high-temperature peaks, and Fig. 7 shows the dependence of Ce-based H_2 consumption at either of the low- or high-temperature peak(s) upon the Ce content. The Ce-based H_2 consumption at the low-temperature peak(s) increased with the decrease in the Ce content and the largest value was attained at 20 mol% of Ce for the GT samples. This phenomenon is interesting because the decrease in Ce content amplifies the redox action of the sample in spite of the fact that Ce plays a main role for the OSC, Other researchers have also reported similar phenomena.[31,34] The H_2 consumption at the high-temperature peak occurred in the Ce content region >60 mol% and increased with the increase in Ce content. The hydrogen consumption per mole Ce, however, was an order of magnitude smaller than that at the low-temperature peak(s). Since low-temperature reducibility is required for practical application, OSC of CeO_2–ZrO_2 solid solution, in a general sense, is associated with the low-temperature peak.[6] The CP samples exhibited the same trend, although H_2 consumption was slightly smaller. It is interesting

Table 1
H_2 consumptions, BET surface areas and crystallite sizes of the samples.

	Calcination time (h)	Peak temp. (°C)	H_2 consumption (mmol/g)	Total H_2 consumption (mmol/g)	H_2 consumption (mmol/Ce mmol)	Total H_2 consumption (mmol/Ce mmol)	BET surface area (m^2/g)	Crystallite size (nm)
GT(20)-800	0.5	496	0.323	0.323	0.215	0.215	57	7^9
GT(20)-800	3	538	0.590	0.590	0.390	0.390	51	7^8
CP(20)-800	0.5	504(261)	0.095(0.162)	0.257	0.063(0.108)	0.171	30	14^8
CP(20)-800	3	542	0.409	0.409	0.270	0.270	23	11^3
GT(50)-800	0.5	507	0.389	0.389	0.115	0.115	47	7^9
CP(50)-800	0.5	487	0.316	0.316	0.093	0.093	41	–
GT(80)-800	0.5	483(746)	0.219(0.111)	0.330	0.044(0.023)	0.067	32	12^3
CP(80)-800	0.5	451(800)	0.280(0.044)	0.324	0.057(0.009)	0.066	56	7^8

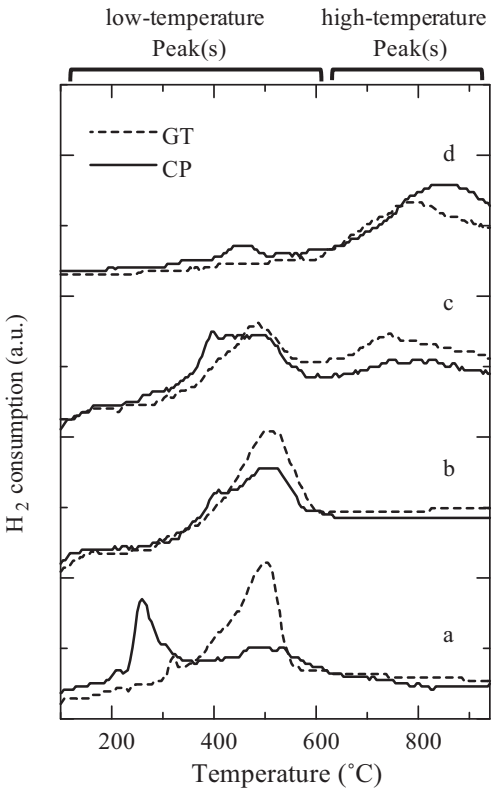

Fig. 6. TPR profiles for GT and CP samples obtained by the calcination at 800 °C for 30 min. Ce mol%: a, 20; b, 50; c, 80; d, 100 [CeO_2].

to note that H_2 consumption of CP(50)-800 was only slightly smaller than that of GT(50)-800 in spite of the fact that phase segregation was apparently observed for the former sample.

The TPR pattern for a single component CeO_2 is rather simple. Yao and Yu Yao have observed two reduction peaks at around 500 °C and 750 °C, and assigned the former peak as the reduction of the surface oxygen, while the latter peak was ascribed to the bulk oxygen reduction.[35] These assignments seem to be generally accepted.[24] Giordano et al. stated that although the high temperature peak is intrinsic to CeO_2, the appearance of the low temperature peak closely depends on the sample history that the material has undergone before TPR experiment.[36]

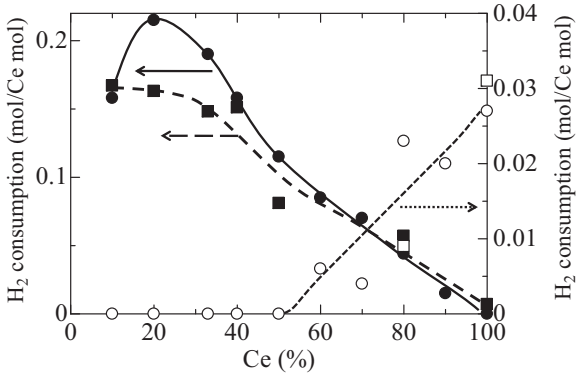

Fig. 7. Effects of Ce content (x) on H_2 consumption of GT(x)-800 (circle) and CP(x)-800 (square) at low temperatures (closed symbols) and high temperatures (open symbols).

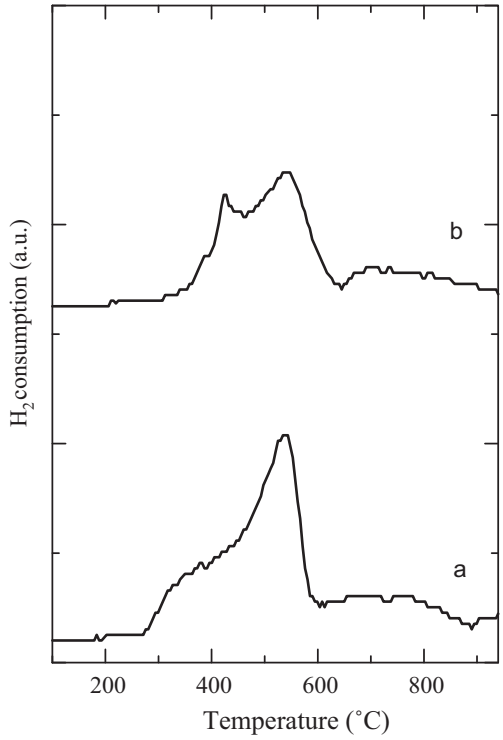

Fig. 8. TPR profiles of (a) GT(20)-800 and (b) CP(20)-800 samples each calcined for 3 h.

Therefore, the reduction peak due to surface oxygen is a subtle matter and whether it occurs or not depends on the nature and history of the CeO_2 samples. Although CP(100) had both low- and high-temperature peaks, GT(100) did not exhibit the low temperature peak, which may be due to relatively low surface area of this sample.

The redox behavior of CeO_2–ZrO_2 solid solutions is complex. Despite decades' investigation, there are still disagreements and controversies about the origin of the redox behavior; therefore, interpretation of the TPR patterns is rather difficult.

As is shown in Fig. 6, two TPR peaks were observed for both GT and CP samples with Ce content of 70–90 mol%, while only the low temperature peak(s) was present for the samples in lower Ce content region. Similar results were reported previously.[24,37] Fornasiero et al.[38] prepared $Ce_{0.5}Zr_{0.5}O_2$ by a citrate method, and found that the sample exhibited a reduction peak at 921 K, while re-oxidation after TPR experiment gave a new reduction peak at ~658 K, besides the 921 K peak. Thus, the number of the peaks and their position differ depending upon the origin of the samples employed; slight differences in the preparation conditions lead to remarkable differences in the TPR profile of CeO_2–ZrO_2 mixed oxide. The low-temperature reduction peak of the $Ce_{0.5}Zr_{0.5}O_2$ sample, nowadays, is explained by formation of κ-$CeZrO_4$ phase formed by reoxidation of pyrochlore-type $Ce_2Zr_2O_7$ phase, which was formed by reduction at high temperatures.[39–42] However, if the formation of the κ-$CeZrO_4$ phase is the sole reason for the low temperature peak of CeO_2–ZrO_2 samples, the low-temperature reduction peak of ZrO_2-rich samples would be associated with the phase segregation. This was not the case (vide infra). The origin of these

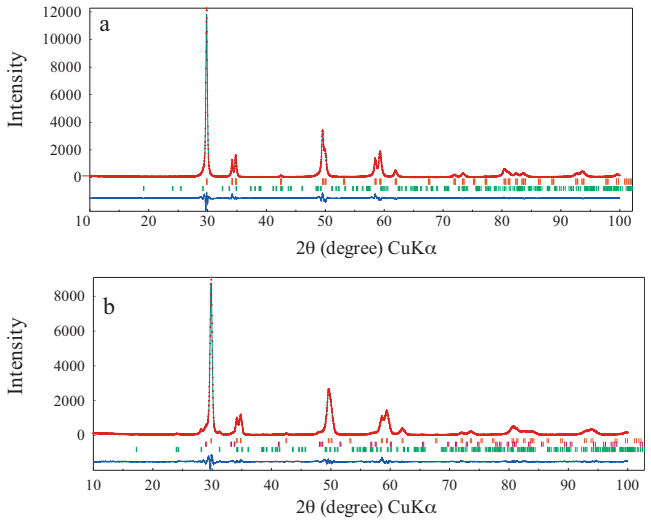

Fig. 9. XRD patterns obtained from Rietveld analysis of GT (a) and CP (b) samples (Ce = 20 mol%) calcined at 1100 °C for 3 h.

reduction peaks, therefore, is not so clearly understood as those for single component CeO_2. Kozolov et al.[43] assigned the low temperature (below 700 °C) peak of $CeO_2/ZrO_2/Al_2O_3$ as the reduction of highly dispersed CeO_2 and the high temperature peak as that of large CeO_2 crystallites. Liotta et al.[44] analyzed the phase composition of a $Ce_{0.6}Zr_{0.4}O_2$ sample prepared by a sol–gel method and found that the pretreatment conditions severely affect the phase composition, thus altering the TPR profiles. In this report, however, we will not discuss further the origin of the TPR peaks but simply compare the physical and chemical properties of the GT and CP CeO_2–ZrO_2 solid solutions. An attention has been focused on the samples with the Ce content of 20 mol% which exhibited the highest oxygen release capacities.

The TPR profiles of the GT and CP samples calcined at 800 °C for 3 h are shown in Fig. 8 and quantitative results are given in Table 1. Prolonged heating increased the H_2 consumption for both the samples, and the GT sample exhibited larger H_2 consumption than the CP sample. Although the CP sample calcined for 30 min had a sharp peak at around 250 °C in addition to a broad peak at 500 °C (Fig. 6a), the former peak disappeared by prolonged calcination and two unresolved peaks appeared at 400–600 °C (Fig. 8b). On the other hand, the TPR profile of the GT sample was essentially unchanged by prolonged heating except for the disappearance of a small shoulder peak at 261 °C (Figs. 6a and 8a). These results indicate that the GT procedure gives homogeneous precursors, while the CP method yields segregated precursors, which requires severe calcination conditions to form stable structures. The crystallite size and surface area of GT(20)-800 scarcely changed after prolonged heating (Table 2). For CP(20)-800, on the other hand, surface area decreased and calculated "crystallite size" also decreased, which can be explained by the progress in phase segregation (see below).

The results for the Rietveld analyses of the XRD patterns of GT(20) and CP(20) calcined at 1100 °C for 3 h are shown in Fig. 9. For the GT sample, the ZrO_2-rich tetragonal phase

Table 2
Results obtained form Rietveld and ICP analyses of the samples.

Sample	Site occupacy			Unit cell parameter (Å)		$c/\sqrt{2}a$	R_{wp}	Ce (at.%)[b]
	4*d*	2*a*		*a*	*c*			
	O	Ce	Zr					
GT(20)-1100[a]	1	0.27	0.73	3.665	5.273	1.017	12.87	24
CP(20)-1100[a]	1	0.14	0.86	3.617	5.210	1.019	10.49	20

[a] Refinement was carried out only for $P4_2/nmc$ phase of CeO_2–ZrO_2.
[b] Ce content was measured by ICP analysis.

was contaminated with a small amount of monoclinic ZrO_2, and the calculated mass fractions of CeO_2–ZrO_2 and ZrO_2 were 98% and 2%, respectively. For the CP sample, on the other hand, at least three phases, ZrO_2-rich tetragonal phase (88%), $Ce_{0.5}Zr_{0.5}O_2$ (4%), and monoclinic ZrO_2 (8%), were required to simulate the XRD pattern. Table 2 summarizes the results of Rietveld analysis and the Ce content in the samples determined by ICP-AES analysis. The site occupancy of Ce in GT(20)-1100 was essentially identical with the Ce content determined by ICP-AES analysis. However, CP(20)-1100 had much lower site occupancy of Ce than the GT sample, because of the presence of a Ce-rich phase ($Ce_{0.5}Zr_{0.5}O_2$) in the former sample. Smaller unit cell parameters also support the low Ce content in the solid solution of the CP sample. These results indicate that Ce and Zr ions in the GT samples are homogeneously dispersed as compared with those in the CP samples.

Fig. 10 and Table 3 show the results of the repetitive reduction–oxidation experiment for the samples calcined at 1100 °C. Contrary to the samples calcined at low temperatures (≤800 °C), both GT and CP samples exhibited only a high-temperature peak. Oxidation of the GT sample at 500 °C after the first TPR procedure resulted in a significant change in the TPR profile. The reduction occurred at a low temperature region (300–600 °C) in the second TPR. On the other hand, only a slight shift to lower temperature was observed for the CP sample, and a broad low-intensity peak appeared in the lower temperature range of the second TPR. The XRD patterns of both the GT and CP samples (oxidized form) after the third reduction–oxidation cycle were the same as those shown in Fig. 9.

The shift of the reduction peak by repeated reduction–oxidation procedures has been reported by other researchers.[34,38,43–46] However, reduction temperature depends on the temperature of re-oxidation.[47] When re-oxidation of a reduced $Ce_{0.5}Zr_{0.5}O_2$ sample was carried out at 700 K, subsequent reduction occurred at lower temperature than the antecedent reduction, while re-oxidation at high temperature (1273 K) restored the high temperature reduction peak. Although their textual properties associated with the structural modifications occurring in the bulk or surface are assumed to be the factors,[34] details of the behavior of CeO_2–ZrO_2 solid solutions on the reduction–oxidation treatment have not yet understood, and therefore, accumulation of the empirical results is required.

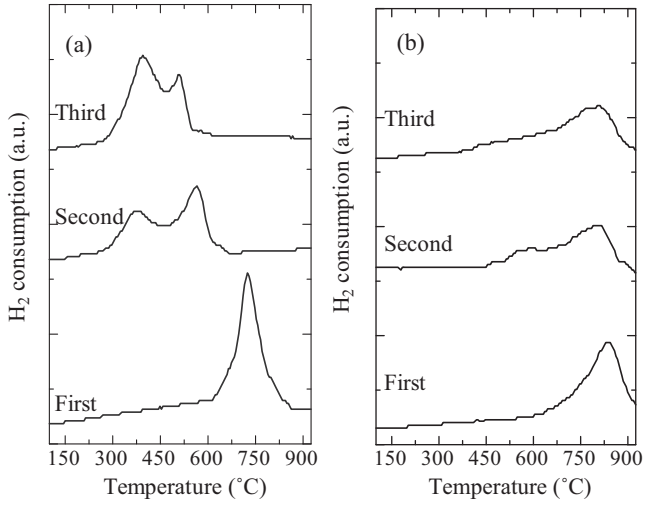

Fig. 10. TPR profiles of (a) GT(20)-1100 and (b) CP(20)-1100 in the repetitive reduction–oxidation experiment.

Homogeneity of CeO_2–ZrO_2 solid solutions is a crucial factor to increase their OSC capacity, although the presence of nanodomains of Ce-rich and Zr-rich phases that cannot

Table 3
H_2 consumptions, BET surface areas and crystallite sizes of the samples.

	Peak temp. (°C)	H_2 consumption (mmol)	H_2 consumption (mmol/Ce mmol)	BET surface area (m^2/g)	Crystallite size (nm)
GT(20)-1100					
First	725	0.590	0.39	1	53
Second	375,564	0.520	0.35		
Third	398,508	0.519	0.35		53[a]
GT(20)-1100					
First	839	0.356	0.24	1	32
Second	798	0.318	0.21		
Third	798	0.299	0.24		25[a]

[a] The crystallite size of the sample after third oxidation process.

be detected by conventional diffraction analysis[47,48] in apparently homogeneous sample cannot be ruled out. The distorted environment around Ce and Zr ions derived from the ordered (homogeneous) solid solution is assumed to be the cause for the favorable low-temperature reduction properties.[6,49] The CeO_2–ZrO_2 samples synthesized by the GT process have highly homogeneous structure as compared with CeO_2–ZrO_2 prepared by CP method, thus exhibiting favorable oxygen transfer properties.

4. Conclusions

In a low Ce content region, the glycothermal reaction of Ce acetate and Zr alkoxide directly yielded CeO_2–ZrO_2 solid solutions. The CeO_2–ZrO_2 solid solution with 20 mol% Ce content obtained by the GT method and subsequent calcination had the largest surface area of the samples in the whole Ce/Zr composition range irrespective of the calcination temperature (500 °C: 125 m^2/g, 800 °C: 57 m^2/g). This sample was composed of spherical particles with 1–2 μm diameter; each sphere was composed of primary particles with about 10 nm size. The oxygen release capacity of CeO_2–ZrO_2 solid solution synthesized by the GT method was much larger than that prepared by the CP method. The CeO_2–ZrO_2 solid solution with 20 mol% Ce content exhibited the highest oxygen release capacity of the samples in the whole Ce/Zr composition range. From the results of Rietveld analysis, the CeO_2–ZrO_2 solid solution synthesized by the GT process has highly homogeneous structure as compared with that prepared by the CP method. The shift of the reduction peak towards lower temperature by reduction–oxidation procedures was observed in the GT CeO_2–ZrO_2 solid solution, but was not observed for the CP CeO_2–ZrO_2 solid solution. This result also indicates Ce and Zr ions in the GT samples are homogeneously dispersed as compared with those in the CP samples.

References

1. Boaro M, Vicario M, Leitenburg CD, Dolcetti G, Trovarelli A. *Catal Today* 2003;**77**:407.
2. Bedrane S, Descrome C, Duprez D. *Catal Today* 2002;**75**:401.
3. Morikawa A, Kikuta K, Suda A, Shinjo H. *Appl Catal B: Environ* 2009;**88**:542.
4. Kim J-R, Myeong W-J, Ihm S-K. *J Catal* 2009;**263**:123.
5. Kakuta N, Ikawa S, Eguchi T, Murakami K, Ohkita H, Mizushima T. *J Alloys Compd* 2006;**408–412**:1078.
6. Nagai Y, Yamamoto T, Tanaka T, Yoshida S, Nonaka T, Okamoto T, et al. *Catal Today* 2002;**74**:225.
7. Kašpar J, Fornasiero P. *J Solid State Chem* 2003;**171**:19.
8. Eguchi K, Akasaka N, Mitsuyama H, Nonaka Y. *Solid State Ionics* 2000;**135**:589.
9. Suda A, Sobukawa H, Suzuki T, Kandori T, Ukyo Y, Sugiura M. *J Ceram Soc Jpn* 2001;**109**:177.
10. Ozawa M, Kimura M, Isogai A. *J Alloys Compd* 1993;**193**:73.
11. Letichevsky S, Tellez CA, de Avillez RR, da Silva MIP, Fraga MA, Appel LG. *Appl Catal B: Environ* 2005;**58**:633.
12. Rossignol S, Gérard F, Duprez D. *J Mater Chem* 1999;**9**, 1615/.
13. Kozlov AI, Kim DH, Yezerrets A, Andersen P, Kung HH, Kung MC. *J Catal* 2002;**209**:417.
14. Fuentes RO, Baker RT. *J Phys Chem C* 2009;**113**:914.
15. Kolko VP, Kriventsov VV, Kochubey DI, Zyuzin DA, Moroz EM, Sadykov VA, et al. *Nucl Instrum Methods Phys Res Sect A* 2007;**575**:91.
16. Lamas DG, Juárez RE, Lascalea GE, Walsöe de Reca NE. *J Mater Sci Lett* 2001;**20**:1447.
17. Grover V, Chavan SV, Sastry PU, Tyagi AK. *J Alloys Compd* 2008;**457**:498.
18. Cabañas A, Darr JA, Lester E, Poliakoff M. *J Mater Chem* 2001;**11**:561.
19. Inoue M, Otsu H, Kominami H, Inui T. *J Am Ceram Soc* 1991;**74**:1452.
20. Hosokawa S, Tanaka Y, Iwamoto S, Inoue M. *Adv Sci Technol* 2006;**45**:691.
21. Inoue M, Nishikawa T, Nakamura T, Inui T. *J Am Ceram Soc* 1997;**80**:2157.
22. Hosokawa S, Tanaka Y, Iwamoto S, Inoue M. *J Mater Sci* 2008;**43**:2276.
23. Inoue M, Sato K, Nakamura T, Inui T. *Catal Lett* 2000;**65**:79.
24. Rumruangwong M, Wongkasemjit S. *Appl Organomet Chem* 2006;**20**:615.
25. Suda A, Yamamura K, Morikawa A, Nagai Y, Sobukawa H, Ukyo Y, et al. *J Mater Sci* 2008;**43**:2258.
26. Zhang HT, Wu G, Chen XH. *Mater Chem Phys* 2007;**101**:415.
27. Kim J-R, Myeong W-J, Ihm S-K. *Appl Catal B: Environ* 2007;**71**:57.
28. Di Monte R, Kašper J, Bradshaw H, Norman C. *J Rare Earth* 2008;**26**:136.
29. Izumi F, Ikeda T. *Mater Sci Forum* 2000;**321**:198.
30. Inoue M, Nishikawa T, Kominami H, Inui T. *J Mater Sci* 2000;**35**:1541.
31. Nakatani T, Okamoto H, Ota R. *J Sol–Gel Sci Technol* 2003;**26**:859.
32. Imamura S, Hamada R, Saito Y, Hashimoto K, Jindai H. *J Mol Catal A: Gen* 1999;**139**:55.
33. Takeguchi T, Furukawa S, Inoue M. *J Catal* 2001;**202**:14.
34. Bernal S, Blanco G, Calvino JJ, Gatica JM, Perez Omil JA, Pintado JM. *Top Catal* 2004;**28**:31.
35. Yao HC, Yu Yao YF. *J Catal* 1984;**86**:254.
36. Giordano F, Trovarelli A, de Leitenburg C, Giona M. *J Catal* 2000;**193**:273.
37. Vidal H, Kašper J, Pijolat M, Colon G, Bernal S, Cordón A, et al. *Appl Catal B: Environ* 2000;**27**:49.
38. Fornasiero P, Kašper J, Graziani M. *Appl Catal B: Environ* 1999;**22**:L11.
39. Otsuka-Yao-Matsuo S, Omata T, Izu N, Kishimoto H. *J Solid State Chem* 1998;**138**:47.
40. Kishimoto H, Omata T, Otsuka-Yao-Matsuo S, Ueda K, Hosono H, Kawazoe H. *J Alloys Compd* 2000;**312**:94.
41. Sakaki T, Ukyo Y, Suda A, Sugiura M, Kuroda K, Arai S, et al. *J Ceram Soc Jpn* 2003;**111**:382.
42. Alessandri I, Bañres MA, Depero LE, Feroni M, Forasiero P, Gennari FC, et al. *Top Catal* 2006;**41**:35.
43. Kozlov AI, Kim DH, Yezerets A, Andersen P, Kung HH, Kung MC. *J Catal* 2002;**209**:417.
44. Liotta LF, Macaluso A, Longo A, Pantaleo G, Martorana A, Deganello G. *Appl Catal A: Gen* 2003;**240**:295.
45. Di Monte R, Kašper J. *J Mater Chem* 2005;**15**:633.
46. Di Monte R, Kašper J. *Catal Today* 2005;**100**:27.
47. Mamontov E, Brezny R, Koranne M, Egami T. *J Phys Chem B* 2003;**107**:13007.
48. Montini T, Speghini A, De Rogatis L, Lorenzut B, Bettinelli M, Graziani M, et al. *J Am Chem Soc* 2009;**131**:13155.
49. Fornasiero P, Montini T, Graziani M, Kašper J, Hungría AB, Martínez-Arias A, et al. *Phys Chem Chem Phys* 2002;**4**:149.